



The study of multipacting in the experimental regions has been conducted using E-CLOUD [11] and considering the following set of parameters and/or assumptions:

1. The maximum SEY is 1.1 or 1.4.
2. We have assumed the elastic reflection to occur as on the copper samples recently measured [12]. Elastic reflection is anyway strongly dependent on the surface roughness more than on the material on which the electrons impinge.
3. The photon flux to the wall for the LHC geometry has been evaluated using the code developed by F. Zimmermann [13]. We expect the photon flux in the straight experimental areas to be sensibly smaller than the one in the arcs.
4. Bunch transverse sizes have been taken at injection and at top energy, both at the interaction points and up to 20m downstream. The study shows, that there is no strong dependence of the electron multipacting on this parameter. This was predictable since for the cases considered, the beam was much smaller than the pipe cross section.
5. The two cases of two beams reaching a selected location simultaneously (25ns bunch spacing and double bunch intensity) and two beams at half distance (12.5ns bunch spacing and single bunch nominal intensity) have been simulated.
6. Geometry variable in steps from the smallest to the largest diameter for each experimental region.
7. The effects of RF traps in enlarged sections of the chambers have not been taken into account.

Table 1. LHC parameters assumed in the electron cloud simulations

|                                  | symbol | value                     |
|----------------------------------|--------|---------------------------|
| bunch proton population          | $N_b$  | $1.05 \times 10^{11}$     |
| bunch spacing                    |        | 7.48 m                    |
| r.m.s. bunch length              |        | 7.5 cm                    |
| proton energy                    |        | 7 TeV                     |
| primary ph-e rate per photon     |        | $2.98 \times 10^{-7}$     |
| Reflectivity                     |        | 10%                       |
| max secondary emission yield     | SEY    | 1.1 and 1.4               |
| energy of max SEY                |        | 300 eV                    |
| energy distr. for sec. Electrons |        | Gaussian                  |
| r.m.s. horizontal beam size      |        | 15.86 - 444 $\mu\text{m}$ |
| r.m.s. vertical beam size        |        | "                         |
| radial half aperture             |        | 22 to 200 mm              |

### 2.3. Simulation results: electron density and flux to the wall

The electron line density ( $e^-/\text{m}$ ) and flux to the wall ( $e^-/\text{s/m}$ ) are displayed in Fig. 2, 3 and 4 for different chamber radii, and for SEY = 1.4. It can be observed that, despite the low value of SEY, there is an electron cloud build up.

Both the rise time and saturation values depend on the chamber radius. No obvious correlation was found.

In Fig. 5, the saturation values of the electron flux to the wall per unit wall area ( $e^-/\text{s}/\text{cm}^2$ ), with SEY = 1.1 and SEY = 1.4 are compared. The saturation levels appear to be more sensitive to a variation of SEY for radii > 70 mm. For the calculations of the residual gas density it was assumed that the electron flux to the wall is a step function, given the shape of the curves and that the two cases considered (simultaneous arrival and half bunch spacing) should correspond to the extreme cases. The values used are shown in Fig. 5, with blue dotted lines.

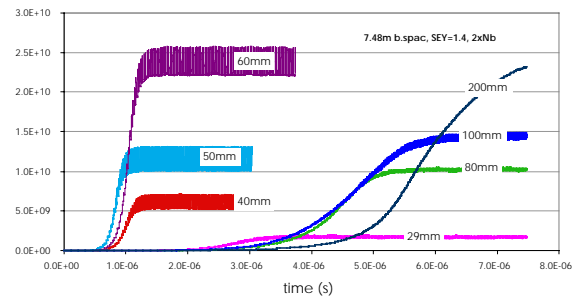


Figure 2: Time evolution of the electron line density ( $e^-/\text{m}$ ) for different chamber radii, for two beams arriving simultaneously (nominal bunch spacing and double bunch current).

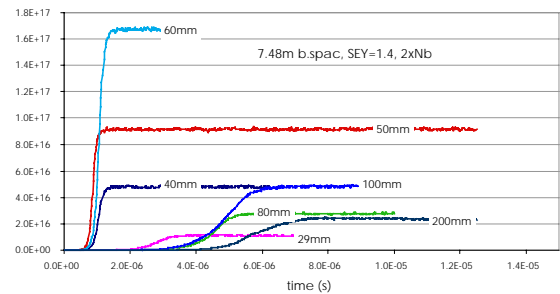


Figure 3: Time evolution of the electron flux to the wall ( $e^-/\text{s}/\text{m}$ ) for different chamber radii, for two beams arriving simultaneously (nominal bunch spacing and double bunch current).

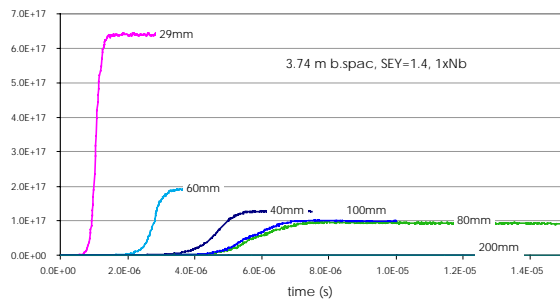


Figure 4: Time evolution of the electron flux to the wall ( $e^-/\text{s}/\text{m}$ ) for different chamber radii, for two beams at half nominal bunch spacing and bunch current.

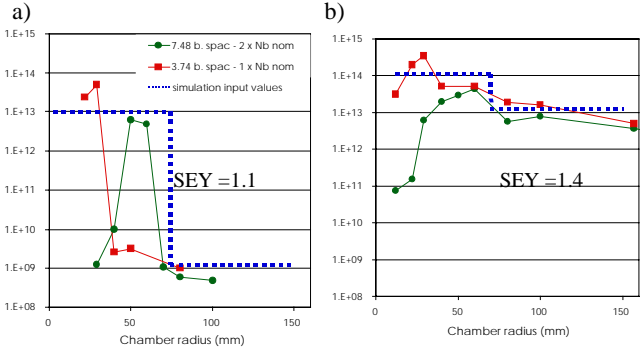


Figure 5: Saturation value of the electron flux to the wall ( $e^-/cm^2$ ) as a function of the chamber radius, and the values used for the calculations of the gas density in the experimental regions. a) SEY = 1.1; b) SEY = 1.4.

#### 2.4. Simulation results: electron impact energy distribution at the wall

The electron impact energy distribution at the wall is displayed in Fig. 6 for the two cases of beams arriving simultaneously and with half nominal bunch spacing. The maximum impact energy varies between 2.5 keV for the latter case and 4.5 keV for simultaneous beams (which corresponds to twice the bunch current). Both figures display an energy range from 0 to 160 eV to show that a non negligible fraction of the electrons impinge on the walls with an energy larger than 10 eV, that is larger than the threshold energy for stimulated gas desorption [6].

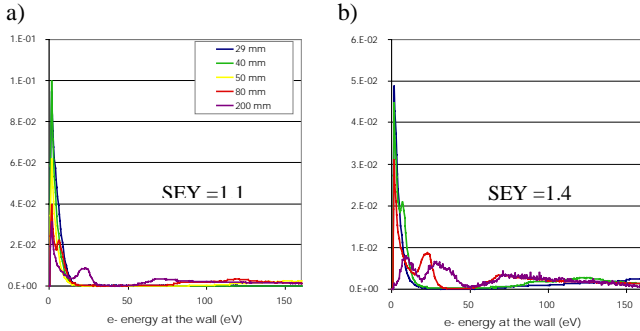


Figure 6: Electron energy distribution at the wall (eV). a) beams arriving simultaneously, with double current. b) beam at half of the nominal bunch spacing and nominal current.

### 3 MOLECULAR DENSITY ESTIMATION IN THE EXPERIMENTAL REGIONS

#### 3.1. Molecular density estimation parameters

As mentioned in the previous section, a large fraction of the electrons impinging on the wall will cause gas desorption. The Electron Stimulated Desorption yield (ESD) depends on the impact energy [6]. The values for ESD used for the estimates of the residual gas density are listed in Table 2 for TiZrV coating [14]. Since the ESD

varies by a factor of  $\sim 2$  between 100 and 300 eV, and given the spread of measured data in the literature, a constant value for all energies was assumed.

Table 2 also contains other parameters relevant for the molecular density estimations, such as the Photon Stimulated gas Desorption (PSD) from TiZrV NEG coating and its sticking coefficients. It should be noted that the desorption yields from NEG coating are reached with other LHC materials after a long conditioning (about 1 year LHC beam time).

Table 2. LHC parameters assumed in the residual gas density estimations for the TiZrV NEG coating

| Desorption Yield                         | H <sub>2</sub>       | CH <sub>4</sub>      | CO                    | CO <sub>2</sub>       |
|--|----------------------|----------------------|-----------------------|-----------------------|
| PSD <sup>i</sup>                         | $2.5 \times 10^{-7}$ | $2.5 \times 10^{-9}$ | $1.25 \times 10^{-8}$ | $1.25 \times 10^{-8}$ |
| ESD <sup>ii</sup> [14]                   | $2.0 \times 10^{-4}$ | $5.0 \times 10^{-6}$ | $1.0 \times 10^{-4}$  | $1.0 \times 10^{-4}$  |
| <i>Sticking Coefficient</i>              |                      |                      |                       |                       |
| Freshly activated NEG <sup>iii</sup> [7] | $5.0 \times 10^{-3}$ | 0                    | $1.0 \times 10^{-1}$  | $1.0 \times 10^{-1}$  |
| Cycled NEG <sup>iv</sup> [7]             | $5.0 \times 10^{-4}$ | 0                    | $1.0 \times 10^{-2}$  | $1.0 \times 10^{-2}$  |

<sup>i</sup> Corrected for grazing incidence (factor of 5 larger at grazing incidence [15] than perpendicular incidence [16]) and considering the expected 12eV critical energy at the LHC interaction regions [17].

<sup>ii</sup>  $\sim 500$ eV incident energy.

<sup>iii</sup> Corresponding to SEY = 1.1.

<sup>iv</sup> Cycled = exposed to air at atmospheric pressure and reactivated several ( $\sim 10$ ) times. SEY = 1.4.

#### 3.2 Results

The density profiles for the ATLAS and CMS (with TOTEM) experimental beam pipe are presented in Fig. 7 and 8. The 'static' density (Fig. 7.1 a) and 8.1, a)) is estimated for a freshly activated NEG coating and is compared to the expected values during proton beam operations (SEY = 1.1, Fig. 7.1 b) and 8.1, b)). It should be noted that the major contribution to the gas density is given by electron induced desorption, since photon induced desorption is at least 2 orders of magnitude smaller. In both cases, the main gas species is methane. The ATLAS beam pipe has a smaller cross section, which accounts for the higher density of CH<sub>4</sub>, whose pumping is conductance limited.

After the NEG coating has been exposed to air at atmospheric pressure (due for example to maintenance works) and reactivated for about 10 times, the  $\delta_{\max}$  increases to  $\sim 1.4$  with a consequent increase of the electron cloud activity, as detailed in section 2. At the same time, the sticking coefficients, and therefore the distributed pumping, is reduced to about one tenth of the initial value. Both phenomena lead to a further increase in the molecular density as shown in Fig. 7.2 and 8.2. The hydrogen density is now comparable to that of methane,

since the distributed pumping speed for hydrogen is low, while the pumping of methane is not affected by the NEG deterioration.

Note that, beyond 22 m from the IP, the surface is supposed to be at cryogenic temperature. Here, the distributed pumping is effective for methane, but lower than the NEG pumping for the other gas species.

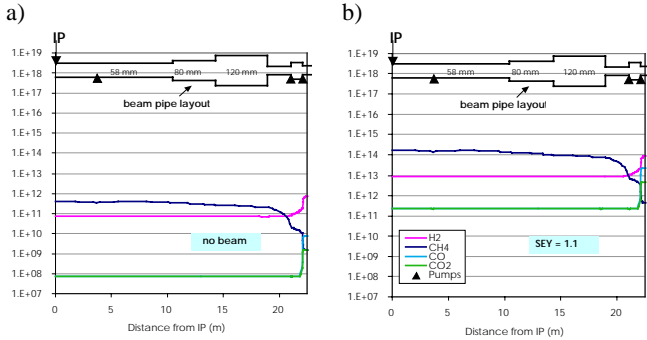


Figure 7.1 : ATLAS experiment. Molecular density distribution (molecules/m<sup>3</sup>) as a function of the distance from the experiment interaction point (IP) for a freshly activated TiZrV NEG coating. a) : no running beam (static). b) : density rise due to electron desorption (main contribution) with SEY = 1.1.

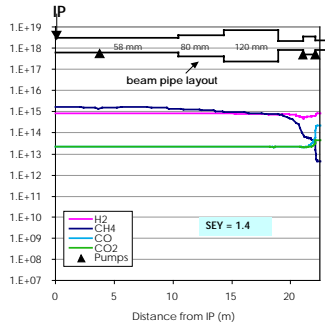


Figure 7.2 : ATLAS experiment. Molecular density distribution (molecules/m<sup>3</sup>) as a function of the distance from IP. The pressure increase due to electron desorption (main contribution) with SEY = 1.4 and 1/10 of NEG pumping.

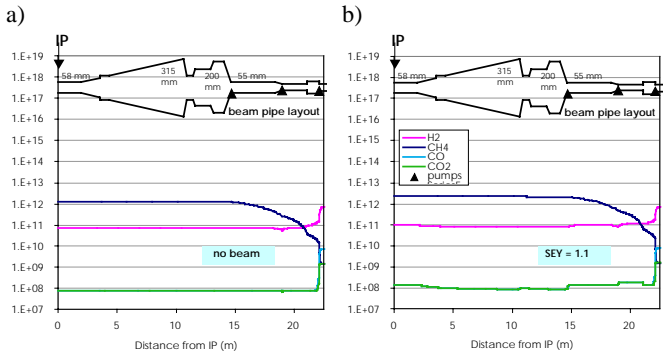


Figure 8.1 : CMS experiment. . Molecular density distribution (molecules/m<sup>3</sup>) as a function of the distance from the IP for a freshly activated TiZrV NEG coating. a) : no running beam (static). b) : density rise due to electron desorption (main contribution) with a SEY = 1.1.

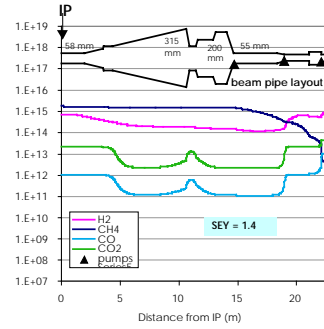


Figure 8.2 : CMS experiment. Molecular density distribution (molecules/m<sup>3</sup>) as a function of the distance from the experiment interaction points (IP). The density increase due to electron desorption (main contribution) is shown for a SEY = 1.4 and 1/10 of the initial NEG pumping.

The profile of the CO and CO<sub>2</sub> gas density in the CMS geometry results from a larger electron flux to the wall in the smaller cross sections (as detailed in Sect. 2.3) and a reduced NEG pumping (which is proportional to the pipe surface area).

#### 4. BENCHMARKING

If the quantitative results of the electron cloud simulations are correct, the main contribution to the residual gas density comes from electron induced gas desorption, as it was explained in the previous section. Since these values are used to assess the validity of the experimental beam chambers design, benchmarking of the simulation results against experimental data is urgently needed. For example, for the CMS experiment, the background noise corresponding to the density levels estimated for SEY = 1.4 is very close to the maximum value the detector can tolerate [18].

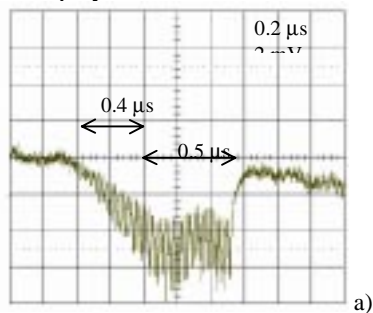
In this section, preliminary results of the electron cloud code benchmarking are presented. The time evolution curves of the electron build-up signal [19] (negative voltage) during experiments in the CERN SPS with LHC type proton beam (25 ns bunch spacing) are compared with the simulation results. The data cannot be converted into number of electrons collected by the pick-up per second, because the instrument was not calibrated prior to the run. In Fig. 9.a) the electron build-up was measured with a train of 72 bunches,  $8.3 \times 10^{10}$  protons/bunch. The pressure measured was about  $2 \times 10^{-7}$  Torr.

The input data for the simulations that best reproduce the experimental data are listed in Table 3. It was assumed that the primary electrons are created by ionisation of the residual gas by the proton beam, as it should be in the SPS. The beam structure and the values assumed for the gas pressure were the same as recorded during the experiments.

Table 3. LHC parameters assumed in the electron cloud simulations for the benchmarking

|                                  | value  |
|----------------------------------|--|
| bunch proton population          | $8.3 \times 10^{10}$                           |
| bunch spacing                    | 7.48 m   |
| r.m.s. bunch length              | 30 cm  |
| proton energy                    | 26 GeV   |
| residual gas pressure            | $2 \times 10^{-7}$ and $4 \times 10^{-8}$ Torr |
| gas ionisation cross section     | 2 MBarn  |
| max secondary emission yield     | 1.6  |
| energy of max SEY                | 300 eV   |
| energy distr. for sec. electrons | Gaussian                                       |
| r.m.s. horizontal beam size      | 444 $\mu\text{m}$                              |
| r.m.s. vertical beam size        | "  |
| radial half horizontal aperture  | 76 mm  |
| radial half vertical aperture    | 17.5 mm  |

The time evolution of the experimental data are well reproduced by the simulations. In Fig. 9.a) the flux of electrons incident on the pick up is plotted as a function of time. In Fig. 9.b), the electron line density resulting from the simulations is displayed.



Courtesy of M. Jimenez [19]

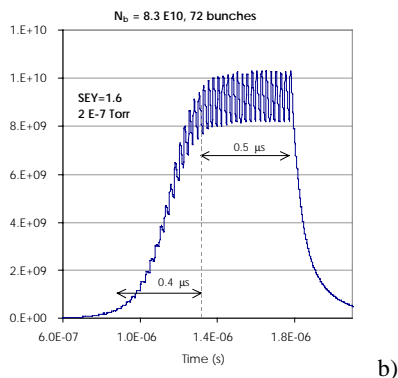


Figure 9: Time evolution with a train of 72 bunches. The experimental data (electron flux to the wall, a) are compared to simulation results (electron line density, b).

## 5 CONCLUSIONS AND FUTURE WORK

The variation of the electron cloud activity with radius (as for the LHC experimental beam pipe geometry) and SEY characteristic of TiZrV NEG coating have been simulated using ELOUD. The results of the simulations

have been used as input to estimate the residual gas density in the interaction regions during proton beam running. It was found that, despite the low SEY of the TiZrV NEG coating after activation, the levels of electron flux to the wall at saturation can induce a gas desorption which will dominate the residual gas density.

Benchmarking of the simulation results are promising. Further effort should be put into this to validate quantitatively the code results so as to use it as a design tool.

The effects of the electron cloud on the beam dynamics are to be analysed.

## 6 REFERENCES

- [1] G. Rumolo and F. Zimmermann, CERN-SL-2001-014-AP.
- [2] A. Mathewson, Maui, Hawaii, November 3-9, 1994.
- [3] ALICE Technical Proposal, CERN/LHCC/95-71.
- [4] ATLAS TDR 13, CERN/LHCC/99-01.
- [5] CMS Technical Proposal, CERN/LHCC/94-38.
- [6] G. Vorlaufer, N. Hilleret, F. Billard, CERN Vac. Tech. Note 00-32.
- [7] C. Benvenuti et al., Vacuum 60 (2001) 57-65.
- [8] C. Scheuerlein et al., CERN EST/2000-07 (SM).
- [9] B. Henrist et al., CERN Vac. Tech. Note 98-08.
- [10] B. Henrist and C. Scheuerlein, CERN Vac. Tech. Note 98-20.
- [11] G. Rumolo and F. Zimmermann, same proceedings.
- [12] V. Baglin, I. Collins, B. Henrist, N. Hilleret, G. Vorlaufer, CERN, LHC-Project-Report-472.
- [13] F. Zimmermann, CERN, LHC Project Report 237 (2000).
- [14] C. Benvenuti, P. Chiggiato, F. Cicoira, V. Rouzinov, Vacuum 50 N. 1-2 (1998) 57-63.
- [15] O. Gröbner, A.G. Mathewson, H. Störi, P. Strubin, R. Souchet, Vacuum 33, N. 7 (1983) 397-406
- [16] V. Baglin, C. Benvenuti, P. Costa Pinto, P. Chiggiato, N. Hilleret, A. Rossi, presented at IVC 15, San Francisco, Nov 2001.
- [17] J. Gómez-Gofi et al., J. Vac. Sci. Technol. A 12(4) Jul/Aug 1994.
- [18] M. Huhtinen, CMS-TOTEM beam pipe EDR, CERN, April 2002.
- [19] M. Jimenez et al., proceedings of 11<sup>th</sup> Chamonix workshop, 2001.